Journal of Neuroinflammation

RESEARCH Open Access

Lactylation of histone by BRD4 regulates astrocyte polarization after experimental subarachnoid hemorrhage

Fan Zhang[1,2†], Jian Zhou[1,2†], Peng Lu[1,2†], Xianhui Zhang[2], Lei Yang[1,2], Jinpeng Wu[1,2], Lihan Zhang[2], Lifang Zhang[4], Jinwei Pang[1], Huangfan Xie[2,3], Bingqing Xie[2,3], Yong Jiang[1,2,3,4*] and Jianhua Peng[1,2,5*]

Abstract

Under subarachnoid hemorrhage (SAH) conditions, astrocytes undergo a marked intensification of glycolytic activity, resulting in the generation of substantial amounts of lactate to maintain the energy demand for neurons and other brain cells. Lactate has garnered increasing attention in recent years because of its emerging role in critical biological processes such as inflammation regulation and neuroprotection, particularly through its histone lactylation. Bromodomain-containing protein 4 (BRD4) plays a crucial role in maintaining neural development and promoting memory formation in the central nervous system. Nonetheless, the function and regulatory mechanism of BRD4 and histone lactylation in astrocytes following SAH remain elusive. Our findings indicate that BRD4, a crucial epigenetic regulator, plays a definitive role in histone lactylation. Both in vitro and in vivo, these results demonstrated that targeted silencing of BRD4 in astrocytes can significantly reduce H4K8la lactylation, thereby aggravating the A1 polarization of astrocytes and ultimately affecting the recovery of neural function and prognosis in mice after SAH. In summary, BRD4 plays a pivotal role in modulating astrocyte polarization following SAH via histone lactylation. Targeting this mechanism might offer an efficient therapeutic strategy for SAH.

Keywords Subarachnoid hemorrhage, Histone lactylation, Astrocytic polarization, Bromodomain-containing protein 4

Introduction

Subarachnoid hemorrhage (SAH) is a major global public health threat, with an annual incidence rate of approximately 6.1 per 100,000 worldwide [1]. Currently, the management of SAH primarily emphasizes the treatment of secondary complications [2]. This approach has provided a certain degree of assistance in improving the quality of life of patients. With the accelerated aging of the global population, the public health burden caused by SAH is becoming increasingly severe [3]. The urgent need to find new brain protection measures is paramount.

Astrocytes play a significant role in neural development, nutritional support, and metabolic regulation in the healthy central nervous system (CNS) [4, 5].

†Fan Zhang M.S., Jian Zhou M.S. and Peng Lu M.S. contributed equally to this work.

*Correspondence:
Yong Jiang
jiangyong@swmu.edu.cn
Jianhua Peng
pengjianhua@swmu.edu.cn
[1]Department of Neurosurgery, The Affiliated Hospital, Southwest Medical University, NO. 25 of Taiping Street, Luzhou, Sichuan 646000, China
[2]Laboratory of Neurological Diseases and Brain Function, The Affiliated Hospital, Southwest Medical University, Luzhou, China
[3]Institute of Brain Science, Southwest Medical University, Luzhou, China
[4]Sichuan Clinical Research Center for Neurosurgery, The Affiliated Hospital, Southwest Medical University, Luzhou, China
[5]Academician (Expert) Workstation of Sichuan Province, The Affiliated Hospital, Southwest Medical University, Luzhou, China

However, under acute or chronic adverse conditions, such as acute ischemic stroke (AIS), Alzheimer's disease (AD) and Huntington's disease (HD), astrocytes exhibit a reactive state and transform into A1 and A2 subtypes [6–9]. In essence, the A1 subtype of astrocytes is harmful, as they can release proinflammatory cytokines that exacerbate neuroinflammation and ultimately lead to neuronal death [10]. However, the A2 subtype exerts protective effects through the upregulation of the expression of certain neurotrophic factors. Consistent with our previous findings, blocking A1 polarization of astrocytes after SAH has neuroprotective effects [11]. Therefore, targeting the phenotypic transformation of astrocytes represents a promising strategy for treating SAH.

The glycolytic pathway in astrocytes abnormally intensifies to sustain the high energy demand of the brain under pathological conditions [4, 12, 13]. Consequently, a substantial amount of lactate is generated and transported to neurons via the lactate shuttle, aiming to supply neurons with energy to combat adverse stimuli and maintain homeostasis [14, 15]. Clinical studies have revealed that elevated lactate levels in extracellular fluid and serum following SAH are often predictive of an unfavorable prognosis [16, 17]. Conversely, lactate has been proposed as a potential therapeutic option for SAH [18]. This controversy may stem from long-standing misunderstandings surrounding the functions of lactate. In 2019, Zhang et al. demonstrated the existence of histone lysine lactylation (Kla). Lactate can promote the transition of macrophages from an inflammatory phenotype to a homeostatic phenotype through lactylation [19]. Research has discovered that lactate, as a modifying group, directly binds to the lysine residues of histones, forming histone lactylation modification, which regulate protein function and promote the transcription of specific genes. This process has been implicated in the modulation of various diseases, including cancer, myocardial infarction, and Alzheimer's disease [20–22]. Our recent research further corroborated the close association between Kla and mitochondrial energy metabolism following AIS [23].

Bromodomain-containing protein 4 (BRD4), an essential member of the bromodomain and extra-terminal domain (BET) family, possesses two bromodomains capable of recognizing lysine residues [24] and is closely related to various physiological and pathological processes [25]. BRD4 functions as an epigenetic reader for histone acetylation [24], which is crucial in activating and elongating gene transcription [26–28]. Lactylation and acetylation share similar occurrence processes and are regulated by epigenetic factors [29, 30]. However, the association between BRD4 and lactylation remains elusive. In the central nervous system, BRD4 is expressed primarily in neurons and astrocytes, where it plays a pivotal role. Broadly inhibiting BRD4 can alleviate neuroinflammation and oxidative stress after acute ischemic stroke while maintaining the integrity of the blood-brain barrier [31]. Conversely, other studies have shown that loss of BRD4 leads to abnormal development of the neural crest [32] and memory deficits in mice [26]. These reports suggest the dual nature of BRD4's function and emphasize the necessity for further exploration. Nonetheless, the involvement of BRD4 in astrocytes following SAH remains ambiguous.

This study investigated the intricate role of BRD4 and histone lactylation after SAH. Our findings showed that lactylation critically regulated astrocyte polarization. Knocking down BRD4 in astrocytes reduced lactylation, particularly H4K8la, which in turn exacerbated A1 polarization, increased neuronal death and worsened functional outcomes after SAH. Targeting lactylation and BRD4 regulation is valuable for the development of neuroprotective drugs.

Materials and methods

Animals

For this study, 161 adult male C57BL/6J mice, aged between 8 and 12 weeks, weighing 16 to 25 g, and sourced from Chengdu Dashuo Laboratory Animal Co., Ltd., were utilized. All animal experiments conducted in this study were approved by the Animal Committee of the Ethics Committee of Southwest Medical University (Approval Number: 20220223-010). All experimental procedures were performed in accordance with the National Institutes of Health guidelines for the Care and Use of Laboratory Animals. The mice were housed in a controlled environment with a 12-hour light/dark cycle, maintained at a temperature of 22 °C, and had free access to food and water. The experimental mice were randomly and blindly assigned to different groups. The animal experimental design is listed in Supplementary Figure S1.

Cell culture and treatment

The HT22 cell line, derived from mouse hippocampal neurons, was obtained from Procell Life Science & Technology. The C8D1A mouse astrocyte cell line was purchased from the American Type Culture Collection (ATCC; Rockville, MD, USA). The cells were cultured in Dulbecco's Modified Eagle Medium (DMEM) supplemented with 10% fetal bovine serum (FBS), 100 U/mL penicillin and 100 μg/mL streptomycin, and incubated in a culture chamber at 37 °C with 5% CO_2. Using 10 μM Oxygenated hemoglobin (OxyHb), dissolved in DMEM, to stimulate C8D1A cells in vitro to mimic subarachnoid hemorrhage injury [11]. Solutions of varying concentrations of 2-deoxy-D-glucose (2DG) and lactate (Sigma-Aldrich, USA) were prepared in DMEM medium for the purpose of stimulating C8D1A cells. Stable BRD4

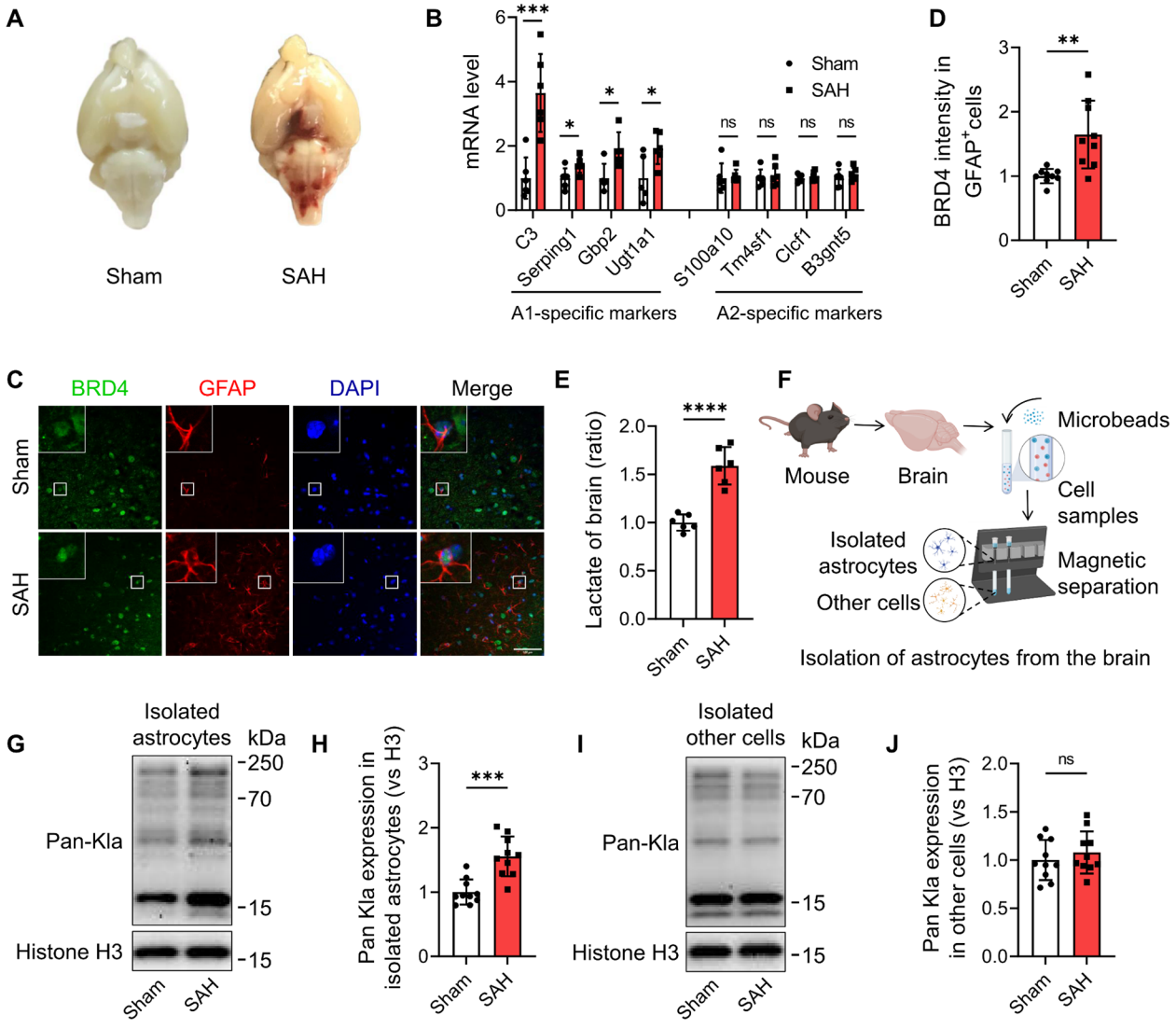

Fig. 1 After 24 h of SAH, astrocytes undergo A1 polarization with elevated levels of BRD4 and lactylation. **(A)** Representative brain images of sham and SAH mice. **(B)** mRNA expression of A1 astrocyte markers (C3, Serping1, Gbp2, and Ugt1a1) and A2 astrocyte markers (S100a10, Tm4sf1, Clcf1, and B3gnt5) in mice subjected to sham and SAH conditions ($n=5$ or 6). **(C-D)** Representative fluorescent images and quantification of BRD4 (green) in astrocytes (GFAP, red). Nuclei were counterstained with DAPI (blue, $n=9$ fields from 3 mice per group). Scale bar, 50 μm. **(E)** Lactate levels in the brains of sham and SAH mice ($n=6$). **(F)** Schematic diagram of astrocyte isolation. **(G-J)** Representative WB images and statistical results of lactylation levels (Indicated by Pan-Kla) in isolated astrocytes and other cells in sham and SAH mice ($n=10$). All values are mean ± SD, $^{*}P<0.05$, $^{**}P<0.01$, $^{***}P<0.001$, $^{****}P<0.0001$, ns, no significant changes

knockdown astrocytes (shBRD4) were obtained through transfection with BRD4 shRNA (OBiO, China), and Control astrocytes (shCtrl) were treated with control shRNA (OBiO, China). Seventy-two hours after transduction, the cells were selected with puromycin, followed by the selection of single-clone cells. The target sequence for BRD4 shRNA was TTCTCCGAACGTGTCACGT, and the Control shRNA sequence was GCGGCAGCTAAG TCTAGATAT. The cell experimental design is listed in Supplementary Figure S1.

Retro-orbital injections of adeno-associated virus (AAV)

The mice were first anesthetized with isoflurane at 3 ml/h for induction and maintained at 1.5 mL/h. Before the injection, they received ophthalmic local anesthesia via proparacaine hydrochloride eye drops (Alcon, USA). Using a 29-gauge insulin syringe, 2×10^{11} vg of astrocyte-targeted AAV (AAV2/PHP. eB-GfaABC1D-mCherry-shCtrl/shBRD4-WPRE) was injected into each mouse. During anesthesia, the body temperature of each mouse was maintained at a constant level using a warming pad [33, 34]. On the basis of the different types of viruses injected, the mice were subsequently categorized

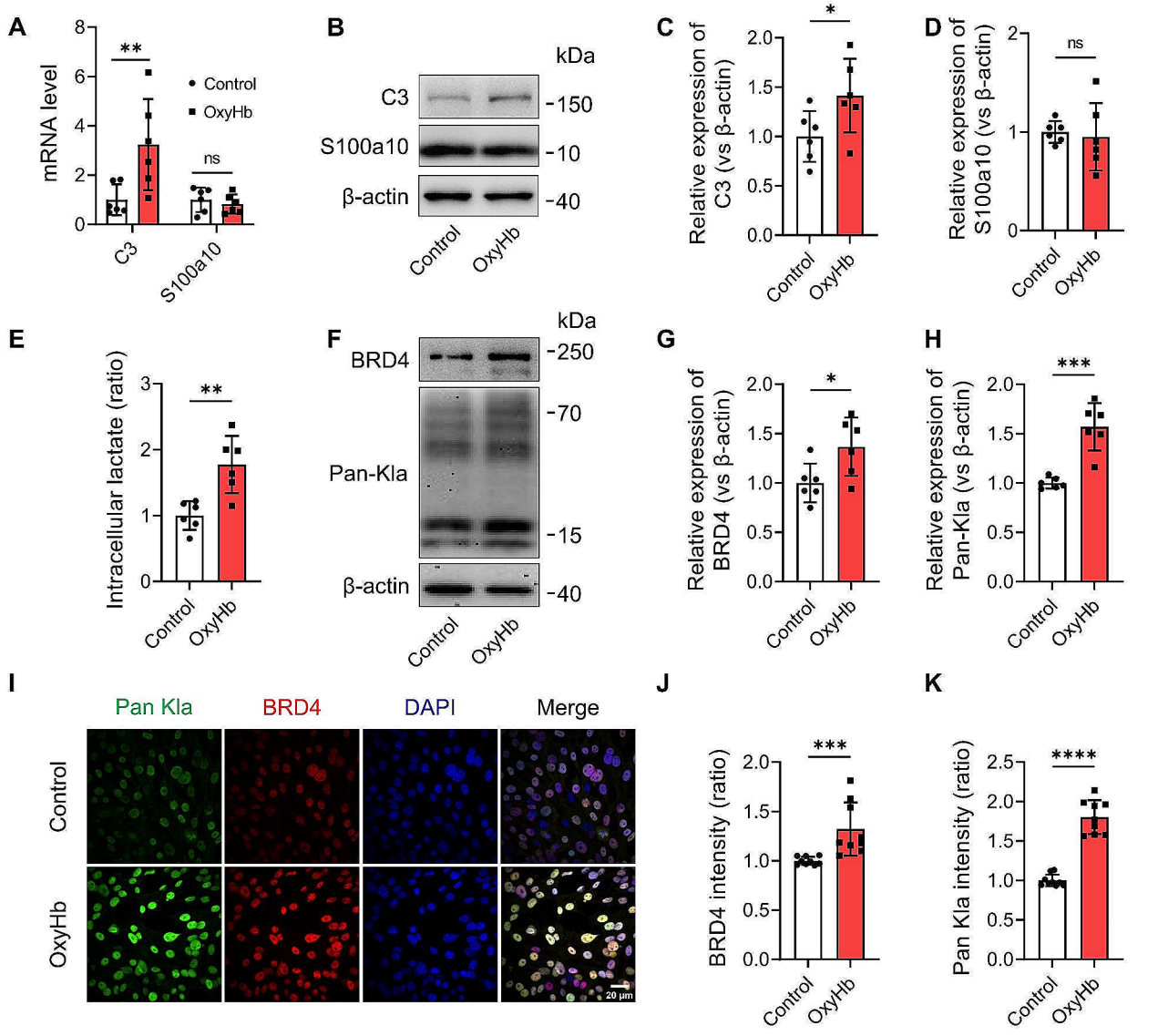

Fig. 2 OxyHb promotes A1 subtype astrocytes and increases BRD4 and lactylation. **(A)** mRNA expression of C3 and S100a10 in astrocytes of the Control and OxyHb groups ($n=6$). **(B-D)** Representative WB images and quantification of C3 and S100a10 in astrocytes of Control and OxyHb groups ($n=6$). **(E)** Lactate levels in astrocytes stimulated with OxyHb ($n=6$). **(F-H)** Representative WB images and quantification of BRD4 and Pan-Kla in astrocytes of Control and OxyHb groups ($n=6$). **(I-K)** Representative fluorescent images and quantification of Pan-Kla (green) and BRD4 (red) expression in astrocytes after OxyHb treatment. Nuclei were counterstained with DAPI (blue, $n=9$). Scale bar, 20 μm. All values are mean ± SD, $^{*}P<0.05$, $^{**}P<0.01$, $^{***}P<0.001$, $^{****}P<0.0001$, ns, no significant changes

into either the Control group or the BRD4 knockdown (BRD4 cKD) group. Three weeks after AAV transfection, the mice were made available for subsequent experimentation.

SAH model

The modified single-clip method was used for intravascular puncture to establish an experimental SAH model in mice [35]. Specifically, mice were anesthetized with isoflurane. The target range for body temperature monitoring and maintenance was 36.5–37.5 °C. An incision was made along the anterior midline of the neck. The subcutaneous tissue, muscle groups, peripheral nerves, and vascular fascia were carefully dissected and separated. The right common carotid artery (CCA), external carotid artery (ECA), and internal carotid artery (ICA) were exposed. A 6−0 monofilament nylon thread was guided from the ECA to the ICA. Once resistance was felt, the thread was advanced 2 mm further and used to puncture the vessel at the point where the anterior and middle cerebral arteries diverged. The Sham groups underwent the same procedure but without vessel puncturing. At

24 h after SAH, the mice underwent neurological deficit scoring and other experimental procedures. In Experiments 1 and 2, 16 mice died within 24 h after SAH. In Experiment 3, one mouse in the SAH-Control group died within 24 h after SAH, whereas two mice in the SAH-BRD4 cKD group died, one within 24 h and the other within 48 h. The grouping and mortality data of the mice are listed in Supplementary Table S1.

Behavioral testing

All behavioral tests were conducted by independent experimenters who were blinded to the group allocation and interventions for testing and analysis.

The Modified Garcia Scale and Beam Balance test were used to assess acute neurological deficits in the mice following SAH [36–38]. The scoring criteria for the Modified Garcia Scale include spontaneous activity (0–3), symmetry of limb movement (0–3), movement of forelimbs (0–3), climbing capacity (1–3), touch of the trunk (1–3), and vibrissa touch (1–3). The Beam Balance test was used to assess the balance and motor ability of the mice. The ability of the mice to walk on a wooden beam for 1 min was scored as: not walk and fall (0); not walk, remains on beam (1); walk, but fall (2); walk less than 20 cm (3); walk beyond 20 cm (4). The Rotarod test was used to evaluate the motor coordination, balance, and fatigue resistance of the mice. For three days prior to the official test, the mice were trained on the rotating rod at 4 rpm/min. On day 4, the rotating rod gradually increased speed from 4 rpm to 40 rpm over 5 min. The test concluded if the mouse fell off or grasped the rod and rotated for 2 rounds without walking on it. The final motor test data represented the average of three such trials [39]. To evaluate the long-term functional outcomes, the Open Field test was utilized to assess the spontaneous locomotor activity of laboratory mice. In brief, before the experiment, the mice were placed in a quiet, lighted environment and then individually introduced into an open-field arena (50×50×25 cm) to explore freely for 6–7 min. Using Smart 3.0 software (Panlab, Spain), their walking distance was analyzed, with a focus on the distance traveled during the final four minutes [40]. The Morris Water Maze test was used to assess the spatial learning and memory abilities of the mice 28 days after SAH injury. The experiment took place in a large, circular pool filled with opaque water at a temperature of 25 ± 2 °C. The maze was deliberately divided into four quadrants, one of which housed a transparent escape platform measuring 10 cm in diameter and situated 1 centimeter beneath the water surface. During the first five training days, the mice were released from one of four starting points and given 60 s to swim freely and find the platform. The mice that did not reach the platform within that time were gently guided there by the experimenter and allowed to rest on it for 10 s. On the sixth day, the platform was removed, and the mice were tested while all other procedures remained the same. The number of times the mice entered the target area were recorded [41].

Isolation of astrocytes from the brain

The mice were anesthetized deeply with pentobarbital sodium and subsequently sacrificed for brain extraction. Following the instructions of the high-activity brain enzyme digestion kit (DHABE-5003, RWD, China) and the single-cell suspension preparation instrument (DSC-400, RWD, China), the brain tissue was prepared as a single-cell suspension. Using Myelin Removal Beads II (130-096-733, Miltenyi Biotec, Germany) and Red Blood Cell Lysis Buffer (R1010, Solarbio, China), myelin and red blood cells were removed from the samples. The total cell pellets were subsequently magnetically labeled with FcR Blocking reagent and Anti-ACSA-2 MicroBeads, adhering strictly to the manufacturer's guidelines. The isolated astrocytes were utilized for WB or RT-qPCR. The purity of the isolated astrocytes was detected by RT-qPCR (Supplementary Figure S2).

RNA isolation and quantitative real-time PCR (RT-qPCR)

Total RNA was extracted from both cultured cells, isolated astrocytes and tissue utilizing the RNA isolater Total RNA Extraction Reagent (Vazyme, China) according to the manufacturer's instructions. A NanoDrop 2000 spectrophotometer (Thermo Fisher Scientific, USA) was subsequently used to accurately determine the concentration of total RNA in each sample. Afterward, the RNA samples were converted into cDNA through reverse transcription using the HiScript®III RT SuperMix for qPCR along with gDNA wiper (Vazyme, China). RT−qPCR was subsequently conducted using the Jena qTOWER real-time PCR system (Jena, Germany) and ChamQTM Universal SYBR® qPCR Master Mix (Vazyme, China). The mRNA expression was normalized to β-actin, and the relative expression was quantified using the $2^{-\Delta\Delta Ct}$ method. The primers used are listed in **Supplementary Table S2**.

Western blot analysis (WB)

The samples were collected and lysed in radio-immunoprecipitation assay (RIPA) buffer supplemented with a protease and phosphatase inhibitor mixture (Beyotime, China). The samples were disrupted using ultrasonication (50% intensity, 5 s, three times), and the reaction was continued on ice for 30 min. After centrifugation at 13,000 g for 10 min, the supernatant was collected. The protein concentration was determined using a BCA kit (Beyotime, China), and the proteins were then denatured in SDS-PAGE loading buffer (Beyotime, China) at 100 °C for 10 min. Equal amounts of protein were loaded onto an SDS-PAGE gel for electrophoresis and then

transferred onto a Polyvinylidene Fluoride (PVDF) membrane. The membrane was blocked with 5% skim milk for 1 h and incubated overnight at 4 °C with the primary antibody: anti-BRD4 (1:1000, ab243862, Abcam, UK), anti-GFAP (1:3000, 16825-1-AP, Proteintech, China), anti-C3 (1:3000, ab200999, Abcam, UK), anti-S100a10 (1:1000, MA8362M, Abmart, China), anti-L-lactyl lysine (1:10000, PTM-1401RM, PTM BIO, China, used to measure the level of pan-lysine lactylation (Pan-Kla)), anti-L-lactyl-histone H4 (Lys 12) (1;2000, PTM-1401RM, PTM BIO, China), anti-L-lactyl-histone H4 (Lys 8) (1:2000, PTM1415RM, PTM BIO, China), anti-L-lactyl-histone H3 (Lys 9) (1:2000, PTM1419RM, PTM BIO, China), anti-L-lactyl-histone H4 (Lys 5) (1:2000, PTM-1407RM, PTM BIO, China), anti-Histone H3 Rabbit (1:10000, PTM-1001RM, PTMBIO, China), anti-Histone H3 Mouse (1:10000, MB9211S, Abmart, China), anti-β-actin Mouse (1:6000, 66009-1-IG, Proteintech, China), and anti-β-actin Rabbit (1:6000, 20536-1-AP, Proteintech, China). Then, the membrane was incubated for 1 h with the appropriate secondary antibody: HRP-conjugated Affinipure Goat Anti-Mouse IgG (H+L) (1:10000, SA00001-1, Proteintech, China) or HRP-conjugated Affinipure Goat Anti-Rabbit IgG (H+L) (1:10000, SA00001-2, Proteintech, China). The signal intensity was visualized using a chemiluminescence kit (Vazyme, China) and analyzed with ImageJ software (NIH). Raw images of western blot are listed in Supplementary Figure S9.

Immunofluorescence (IF) staining

Initially, the mice were euthanized via inhalation of an overdose of isoflurane. Then, the brain tissue was perfused through the heart with PBS and fixed with 4% paraformaldehyde. Following fixation, dehydration was carried out via a sucrose gradient. Using a CM1850 cryostat from Leica (Wetzlar, Germany), the tissue was precisely sliced into 10 μm thick coronal sections. Before the experiment, the brain tissue slices were allowed to warm at room temperature for 30 min. After incubation in rapid antigen retrieval solution for frozen sections (Beyotime, China) for 5 min, the brain tissue sections were permeabilized with 0.3% Triton X-100 for another 10 min. For 1 h, the brain tissue sections were blocked with 10% goat serum at room temperature. The sections were subsequently incubated overnight at 4 ℃ with the following primary antibodies: anti-BRD4 (1:200, ab243862, Abcam, UK), anti-L-lactyl-histone H4 (Lys 8) (1:200, PTM1415RM, PTM BIO, China), or anti-GFAP (1:500, 3670 S, CST, USA). After being rinsed with PBS on the second day, the sections were incubated with the secondary antibody for 1 h. The secondary antibodies used were as follows: Goat Anti-Rabbit IgG H&L (Alexa Fluor® 488) (1:200, ab150077, Abcam, UK), Goat Anti-Mouse IgG H&L (Alexa Fluor® 488) (1:200, ab150113, Abcam, UK), and Goat Anti-Mouse IgG H&L (Alexa Fluor® 594) (1:200, ab150116, Abcam, UK). Subsequently, DAPI was added to stain the cell nuclei, followed by imaging under a fluorescence microscope with the same experimental parameters. We specifically focused on the cortex and brain tissue surrounding the puncture sites.

Cells were seeded onto a polylysine-coated cell climbing slide placed in a 24-well plate and allowed to adhere to the slide for 24 h before being exposed to OxyHb for another 24 h. Then, the cells were fixed in 4% paraformaldehyde in PBS at room temperature for 15 min. The cells were subsequently washed twice with PBS, each time for 5 min. Afterward, the cells were treated with 0.1% Triton-X 100 at room temperature for 10 min to achieve permeabilization. The subsequent operations were the same as those described above. The primary antibodies used were as follows: anti-BRD4 (1:400, M073541, Abmart, China), anti-L-Lactyl lysine (1:800, PTM-1401RM, PTM BIO, China), anti-C3 (1:200, ab97462, Abcam, UK), and anti-S100a10 (1:100, MA8362M, Abmart, China). The secondary antibodies used were as follows: Goat Anti-Rabbit IgG H&L (Alexa Fluor® 488) (1:400, ab150077, Abcam, UK), Goat Anti-Mouse IgG H&L (Alexa Fluor® 488) (1:400, ab150113, Abcam, UK), Goat Anti-Mouse IgG H&L (Alexa Fluor® 594) (1:400, ab150116, Abcam, UK). DAPI was added to stain the cell nuclei. Imaging was performed via fluorescence microscopy under identical experimental conditions.

Astrocytic morphology analysis

Under pathological conditions, astrocytes first morphologically change their long, thin processes to more ramified, larger ones with elongated processes [12]. Statistical analysis of the number of branches, junctions and endpoints and the length of branches can visually reflect the reactivity of astrocytes [42]. Using ImageJ software (NIH), in conjunction with the Analyze Skeleton (2D/3D) plugin, we conducted a quantitative analysis of the morphological alterations in astrocytes within a biological system. GFAP staining was used to immunolabel the astrocytes, outlining the contours and skeletons of the cell bodies. Relevant data were obtained through analyses conducted using Analyze Skeleton (2D/3D) [43].

Terminal deoxynucleotidyl transferase-mediated dUTP-biotin nick end labeling (TUNEL)

TUNEL staining of brain tissue was performed according to the instructions of the kit (Vazyme, China). After permeabilization of the brain tissue slices, the samples were equilibrated with 1x equilibration buffer for 30 min at room temperature, followed by a one-hour incubation with 50 μL of TdT buffer at 37 °C. The slices were subsequently counterstained with anti-NeuN (1:500, ab104224, Abcam, UK) overnight at 4 °C. The next day,

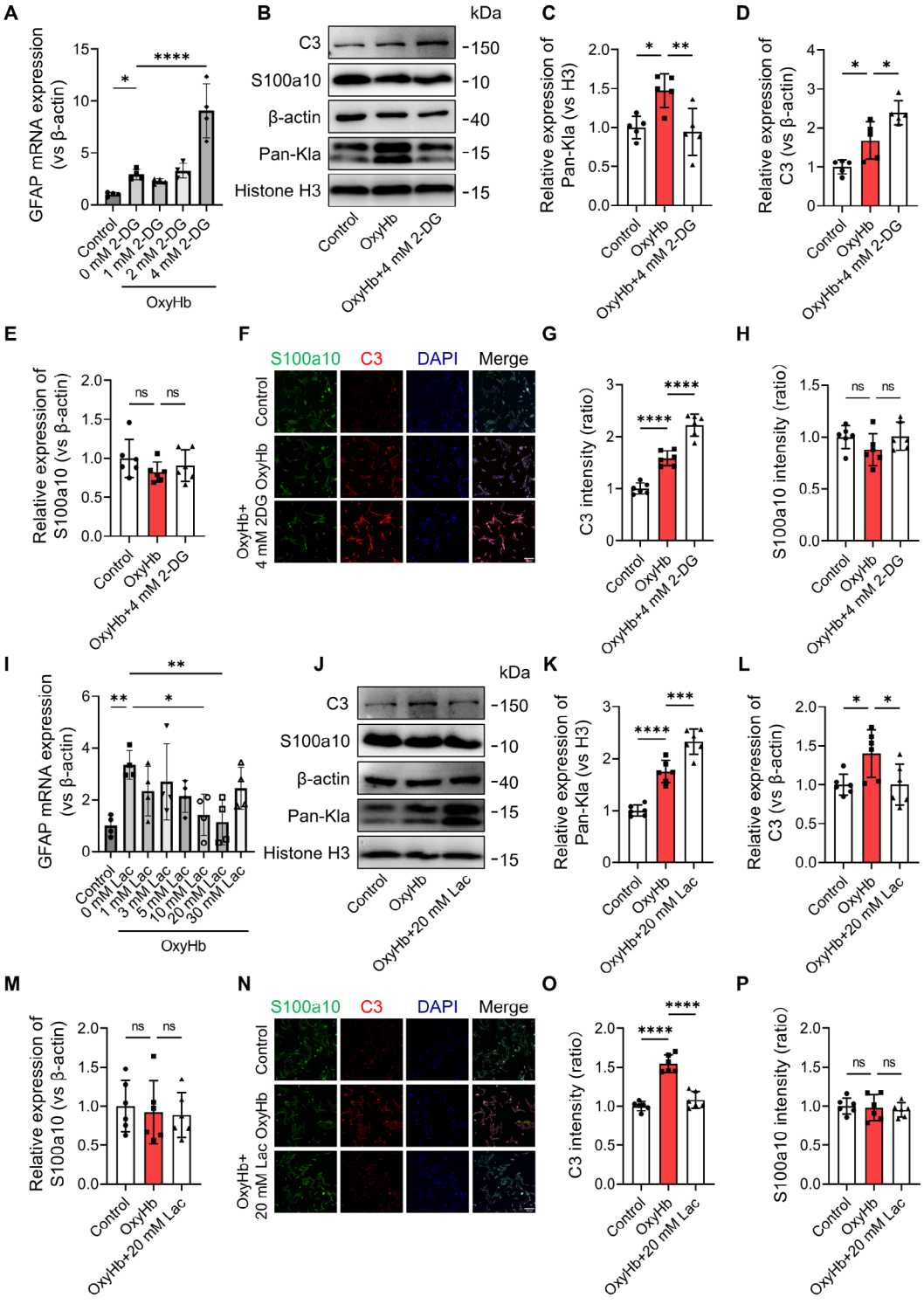

Fig. 3 The A1 polarization of reactive astrocytes following OxyHb is regulated by lactylation. **(A)** mRNA expression of GFAP in astrocytes treated with OxyHb and various concentrations of 2-DG ($n=4$). **(B-E)** Western blot and quantification of Pan-Kla, C3 and S100a10 levels in astrocytes treated with OxyHb and 4 mM 2-DG ($n=5$). **(F-H)** Representative fluorescent images and quantification of C3 (green) and S100a10 (red) expression in astrocytes after OxyHb and 4 mM 2-DG treatment. Nuclei were counterstained with DAPI (blue, $n=6$, scale bar, 100 μm). **(I)** mRNA expression of GFAP in astrocytes treated with OxyHb and varying concentrations of lactate ($n=4$). **(J-M)** Western blot images and quantification of Pan-Kla, C3 and S100a10 levels after treatment with OxyHb and 20 mM lactate ($n=6$). **(N-P)** Representative fluorescent images and quantification of C3 (green) and S100a10 (red) in astrocytes after OxyHb and 20 mM lactate treatment. Nuclei were counterstained with DAPI (blue, $n=6$; scale bar, 100 μm). All values are mean ± SD, $^{*}P<0.05$, $^{**}P<0.01$, $^{***}P<0.001$, $^{****}P<0.0001$, ns, no significant changes

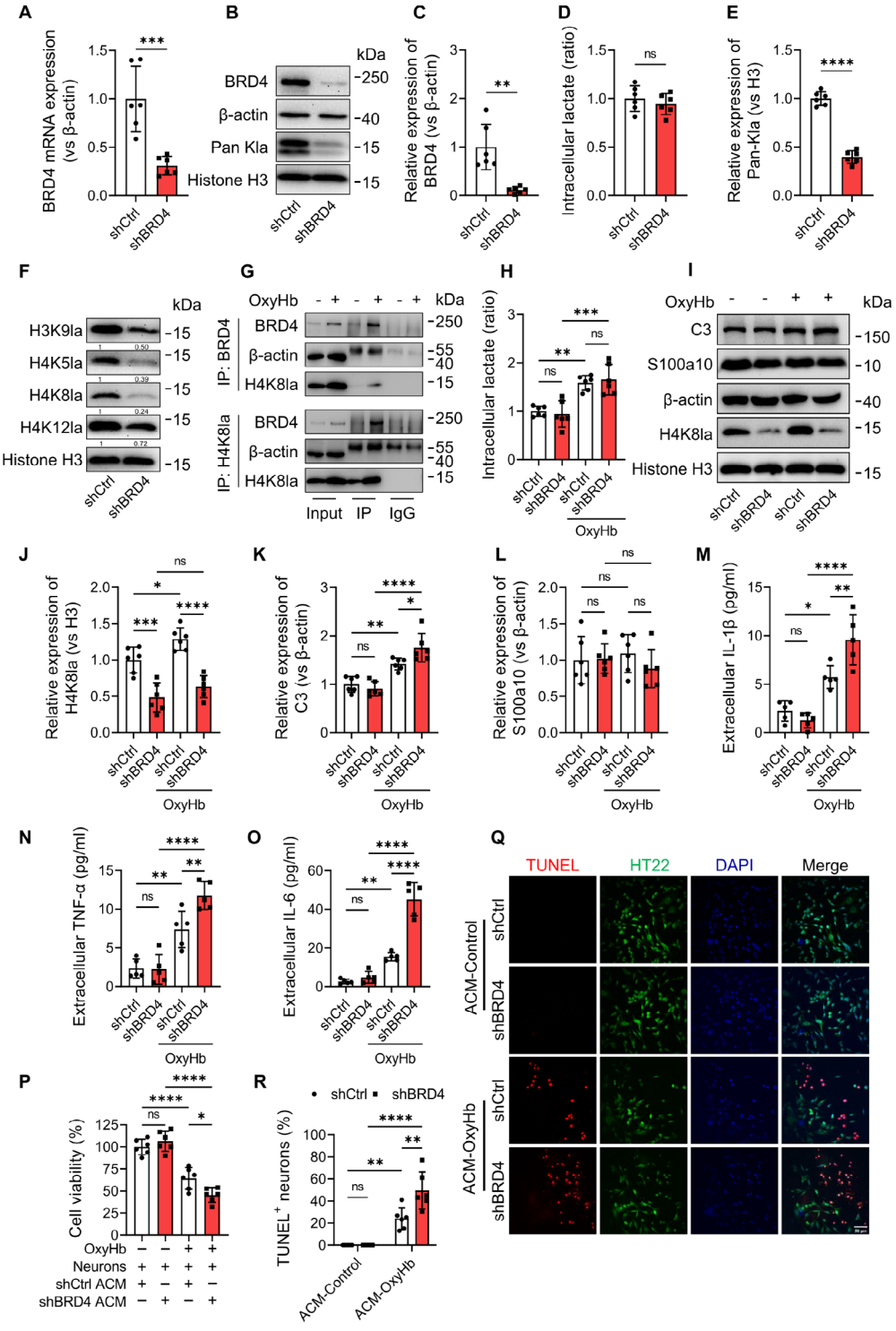

Fig. 4 Knocking down BRD4 aggravates A1 polarization of astrocytes by reducing H4K8la levels. **(A)** BRD4 mRNA expression in shCtrl or shBRD4 cells ($n=6$). **(B, C** and **E)** Western blot showing BRD4 **(C)** and Pan-Kla **(E)** expression in shCtrl or shBRD4 cells ($n=6$). **(D)** Intracellular lactate levels in astrocytes expressing shCtrl or shBRD4 ($n=6$). **(F)** Western blot showing H3K9la, H4K5la, H4K8la, and H4K12la levels in shCtrl or shBRD4 cells ($n=6$). **(G)** BRD4 and H4K8la immunoprecipitation. **(H)** Intracellular lactate in astrocytes expressing shCtrl or shBRD4 when stimulated with OxyHb ($n=6$). **(I-L)** Western blot showing H4K8la **(J)**, C3 **(K)** and S100a10 **(L)** expression in astrocytes expressing shCtrl or shBRD4 when stimulated with OxyHb ($n=6$). **(M-O)** The levels of IL-1β, TNF-α, and IL-6 in the ACM ($n=5$). **(P)** Cell viability of neurons cultured with different ACM ($n=6$). **(Q-R)** Representative fluorescent images and quantification of TUNEL$^+$ neurons cultured with different ACM. Nuclei were counterstained with DAPI (blue, $n=6$; scale bar = 50 μm). All values are means ± SDs, $^*P<0.05$, $^{**}P<0.01$, $^{***}P<0.001$, $^{****}P<0.0001$, ns, no significant changes

the corresponding secondary antibody, Goat Anti-Mouse IgG H&L (Alexa Fluor® 647) (1:200, ab150115, Abcam, UK), was incubated with the samples for 1 h.

For TUNEL staining of HT22 cells, the cells were first fixed with 4% paraformaldehyde at room temperature for 25 min, and the subsequent operations were the same as those described above.

Lactate assay

The lactate concentration in brain tissue and cells was measured using a lactate assay kit (KGT023, KeyGEN BioTECH, China) according to the manufacturer's instructions. The samples were incubated with the working solution for 10 min at 37 °C, the reaction was terminated, and the absorbance was subsequently measured at 530 nm via a spectrophotometer.

Cell viability assay

Using the Cell Counting Kit-8 (HANBIO, China), cell viability was assessed in accordance with the manufacturer's guidelines, and the findings were presented as a percentage relative to the viability of control cells.

BRD4 and H4K8la immunoprecipitation (IP)

Total protein was extracted from cultured astrocytes utilizing a comprehensive lysis buffer mixture. (Cell lysis buffer for immunoprecipitation, P0013; Beyotime, China; protease inhibitor cocktail, HY-K0010; MedChemExpress, USA). Following centrifugation at 13,400 g for 10 min at 4 °C, the protein concentration in the supernatant was measured using a BCA kit. A total of 2,400 μg of protein was incubated with magnetic protein A beads (10002D, Thermo Fisher Scientific, USA) for 30 min at 4 °C, and then, the supernatant was divided into two parts and incubated with control IgG (AC005, ABclonal, China), anti-BRD4 (ab243862, Abcam, UK) and anti-L-lactyl-histone H4 (Lys 8) (PTM1415RM, PTM BIO, China) at 4 °C overnight with constant rotation. The samples were subsequently combined with fresh protein beads and incubated for 6 h at 4 °C. The beads were subsequently washed 3 times to remove nonspecifically bound proteins. Finally, the protein bound to the beads was eluted with 1× loading buffer (FD002, Fude Biological Technology, China) and analyzed by Western blot.

Enzyme-linked immunosorbent assay (ELISA)

The protein levels of IL-1β, TNF-α, and IL-6 were measured via ELISA kits (IL-1β, E-EL-M0037, Elabscience, China; TNF-α, E-EL-M3063, Elabscience, China; and IL-6, E-EL-M0044, Elabscience, China). Frontal cortex tissues from identical regions of the right brain hemispheres of Sham and SAH mice were collected, and the astrocyte-conditioned medium (ACM) stimulated with OxyHB for 24 h was centrifuged at 1000 g for 20 min at 4 °C. The levels of inflammatory cytokines in the brain and ACM were quantified via ELISA kits according to the manufacturer's instructions. The results were normalized to the total protein level of each sample. The results were normalized separately on the basis of the total protein concentration in tissues or cell counts.

Nissl staining

The brain tissues were stained with 0.5% cresyl violet then dehydrated and rinsed with xylene. Nissl bodies and damaged neurons in the frontal cortex, hippocampus, and tissues surrounding the puncture site were observed and photographed.

Statistical analysis

Statistical analysis was performed using GraphPad Prism (Version 9, GraphPad, La Jolla, CA). The Shapiro-Wilk normality test was used to determine the distribution of the data. The data followed a normal distribution and were expressed as mean ± standard deviation (SD). Unpaired 2-tailed Student's t test was used to compare 2 groups, and one- or two-way analysis of variance (ANOVA) followed by Tukey's multiple comparisons test was performed to determine differences among >2 groups. The data, which were not normally distributed, were analyzed through either the Mann-Whitney U test or the Kruskal-Wallis test. Statistical significance was determined when p values were <0.05.

Results

A1 subtype-reactive astrocytes, astrocytic BRD4 expression and lactylation are increased during the early phase of SAH

To clarify the phenotypic changes in astrocytes after SAH, we established experimental models of SAH in mice (Fig. 1A). After 24 h of hemorrhagic injury, as shown by RT-qPCR, the mRNA levels of markers of A1 astrocytes, including C3 (Complement 3), Serping1 (Serpin family G member 1), Gbp2 (Guanylate-binding protein 2) and Ugt1a1 (Uridine diphosphate glucuronosyl transferase 1a1), were increased. However, S100a10 (S100 calcium-binding proteina10), Tm4sf1 (Transmembrane 4 L six family member 1), Clcf1 (Cardiotrophin-like cytokine factor 1) and B3gnt5 (β-1, 3-N-acetylglucosaminyltransferase 5), markers of A2 astrocytes, were expressed at the same levels as those in the sham group (Fig. 1B). For the subsequent experiments, we chose C3 and S100a10 as the specific markers for A1 and A2 astrocytes, respectively. Immunofluorescence staining revealed a significant increase in the expression of BRD4 in $GFAP^+$ cells at 24 h post SAH (Fig. 1C-D, Fig. S5A).

Astrocytes are the energy hub that maintains brain function and are also one of the primary sources of lactate [4]. As shown in Fig. 1E, there was a notable elevation in the lactate levels within the brain tissue after SAH.

Previous studies have shown that lactylation mediated by lactate plays a crucial role in various physiological processes and diseases. To clarify the changes in lactylation in astrocytes, Magnetic Bead Sorting was conducted to isolate these cells (Fig. 1F). Next, Western blot analysis confirmed that the Pan-lysine lactylation (Pan-Kla) in isolated astrocytes was increased after SAH (Fig. 1G-H). However, the lactylation of other cells remained unchanged (Fig. 1I-J). The above data indicate that astrocytes polarized toward the A1 phenotype after SAH, accompanied by increased expression of BRD4 and lactylation. On the basis of these findings, we hypothesized that BRD4 and lactylation play latent roles in the polarization of astrocytes.

OxyHb induces A1 subtype reactive astrocytes and enhanced the expression of BRD4 and lactylation

To confirm this hypothesis, astrocytes were stimulated with 10 μM OxyHb for 24 h [11]. OxyHb enhanced astrocytic A1 polarization. As shown by PCR and WB (Fig. 2A-D), there was notable upregulation of C3 expression, whereas the expression level of S100a10 remained largely unchanged. As expected, OxyHb induced an increase in lactate levels in astrocytes (Fig. 2E). Moreover, both WB and IF staining indicated that the levels of lactylation/Pan-Kla and BRD4 were greater than those in the control groups (Fig. 2F-K). Moreover, as shown in Fig. 2I, BRD4 and Pan-Kla were highly colocalized in the nuclei of astrocytes. These findings suggest a potential association between BRD4 and lactylation. Through these experiments, we found that OxyHb stimulation for 24 h induced A1 subtype reactive astrocytes, increasing the expression and lactylation of BRD4.

A1 polarization of reactive astrocytes following OxyHb is regulated by lactylation

We next designed experiments to explore the role of lactate and lactylation in the phenotypic polarization of astrocytes. OxyHb and different concentrations of 2-deoxy-D-glucose (2-DG, a glycolysis inhibitor) were used to inhibit the production of lactate. These results revealed that low concentrations of 2-DG had no significant effect, whereas 4 mM 2-DG markedly increased the expression of GFAP (Fig. 3A). Subsequent experiments with 4 mM 2-DG revealed that the lactylation of astrocytes was significantly inhibited (Fig. 3B-C), accompanied by a further increase in C3 expression and no change in S100a10 (Fig. 3B and D-E). When C3 and S100a10 were costained, the results obtained were consistent with those described above (Fig. 3F-H, Fig. S3A). Conversely, after the addition of lactate for 24 h, RT-qPCR was used to detect the mRNA level of GFAP. As shown in Fig. 3I, the expression of GFAP was downregulated following lactate treatment, especially in the 20 mM Lac group. Therefore, we chose 20 mM lactate for further investigation. Remarkably, the expression of lactylation was further upregulated (Fig. 3J-K). Notably, lactate suppressed the level of C3, which was elevated in response to OxyHb stimulation (Fig. 3J and L). The impact of lactate treatment on the expression of S100A10 was minimal (Fig. 3J and M). The immunofluorescence results also revealed the same changes (Fig. 3N-P, Fig. S3B). These data indicate that increased lactylation can reduce A1 transformation of astrocytes treated with OxyHb.

Knockdown of BRD4 aggravates A1 polarization of astrocytes by reducing H4K8la levels, subsequently inducing neuronal death following OxyHb

To investigate the role of BRD4 in regulating astrocytic polarization following SAH, we generated BRD4 knockdown C8D1A astrocytes. RT-qPCR and WB both confirmed satisfactory gene silencing efficiency (Fig. 4A-C). The decrease in the intracellular lactate level was minimal, indicating that the glycolytic pathway and lactate production in the astrocytes were not significantly affected by BRD4 knockdown (Fig. 4D). Interestingly, we observed a significant reduction in the level of lactylation after BRD4 interference (Fig. 4B and E). BRD4, an epigenetic regulator, can bind to histone sites such as H3K9, H4K5, H4K8, and H4K12 [24]. WB revealed that the lactylation of multiple histone sites decreased after BRD4 knockdown, with the most pronounced decrease observed in H4K8la (Fig. 4F). Through IP experiments, we validated the direct interaction between BRD4 and H4K8la (Fig. 4G). These results indicate that BRD4 may function in regulating lactylation and H4K8la.

We found that lactylation can regulate the polarization of astrocytes, whereas BRD4 can modulate lactylation. We conducted subsequent experiments to explore the effect of BRD4 knockdown on astrocytic polarization. As shown in Fig. 4H, the shCtrl and shBRD4 groups presented similar increases in lactate levels upon OxyHb stimulation, confirming previous results. We conducted WB to investigate the impact of BRD4 knockdown on the expression of H4K8la, C3, and S100A10 in astrocytes stimulated with OxyHb. As shown in Fig. 4I-L, OxyHb-shCtrl resulted in significant H4K8la upregulation compared with shCtrl, but no such effect was observed in shBRD4 or OxyHb-shBRD4. Furthermore, the protein levels of C3 in the OxyHb-shCtrl group were significantly elevated, and OxyHb-shBRD4 further exacerbated these changes. Similarly, the expression of S100A10 was not affected by the intervention. These results suggest that BRD4 regulates astrocyte A1 polarization through H4K8la following SAH.

The release of proinflammatory cytokines and neurotoxic substances by A1 astrocytes can lead to neuronal death [11]. We measured the content of proinflammatory

cytokines in the astrocyte-conditioned medium (ACM) of the Control-shCtrl, Control-shBRD4, OxyHb-shCtrl, and OxyHb-shBRD4 groups. The concentrations of IL-1β, TNF-α, and IL-6 in the ACM of the OxyHb-shBRD4 group were the highest (Fig. 4M-O). Then, the HT22 cells were further exposed to the ACM for 24 h. Cell viability assays and immunocytofluorescence experiments revealed that OxyHb-shBRD4 ACM further reduced neuronal viability (Fig. 4P) and increased neuronal death (Fig. 4Q-R).

The downregulation of BRD4 enhances the reactivity of astrocytes in mice after SAH

To corroborate the previous findings, astrocytic BRD4 conditional knockdown (BRD4 cKD) mice were generated by retro-orbital injection with GfaABC1D-targeting adeno-associated virus 2 (Fig. 5A). Immunofluorescence was used to verify the signal overlaps between the AAV and astrocytes (Fig. S4). Astrocytes were isolated from the brain, and the BRD4 expression efficiency in these isolated astrocytes was detected via RT−qPCR and WB (Fig. 5B-D). The knockdown efficiency was further validated via immunofluorescence in brain slices (Fig. 5E-F, Figure S5B). Twenty-four hours after SAH, brain lactate levels were increased in both Control and BRD4 cKD mice (Fig. 5G). The WB (samples of isolated astrocytes) and IF results revealed that the expression of H4K8la in the SAH-Control group was greater than that in the sham group, whereas there was no change in the BRD4 cKD group (Fig. 5H-K, Figure S5C). As shown in Fig. 5L and Figure S5D, astrocytes in the cortex of the punctured hemisphere were labeled with GFAP (green). SAH-BRD4 cKD exhibited the strongest fluorescence signal intensity (Fig. 5M). The outline and branching structure of the astrocytes were subsequently delineated. Branches, junctions, end-points, and branch lengths were utilized for a comprehensive analysis of the astrocytic reactivity. Similarly, the SAH-BRD4 cKD group demonstrated superior performance in these key aspects (Fig. 5N). In addition, the same analysis was performed on astrocytes in the frontal cortex and hippocampal, and the results obtained were consistent with those previously results (Fig S6 and S7). These findings suggest that BRD4 plays a pivotal role in modulating astrocyte reactivity, with a direct correlation with diminished levels of H4K8la.

BRD4 knockdown lead to A1 polarization of astrocytes, worsening neuroinflammation and neuronal death

Next, we investigated the astrocytic polarization state by measuring the expression of C3 and S100a10 in the cerebral hemisphere with puncturing (Fig. 6A). Compared with that in the Sham group, the expression of C3 increased significantly after SAH, and the increase was more pronounced when BRD4 was knocked down, whereas no significant changes in the expression of S100a10 was detected (Fig. 6B-C). A1 astrocytes produce abundant proinflammatory cytokines (IL-6, IL-1β, and TNF-α), which exacerbate neuroinflammation following SAH [7]. RT-qPCR revealed that the inflammatory response was the most severe in SAH-BRD4 cKD mice (Fig. 6D-F). The changes in these proinflammatory cytokines were also verified at the protein level through ELISA (Fig. 6G-I). In addition, a strong inflammatory response is unfavorable for neurons. The proportion of $TUNEL^+$ neurons increased in both SAH-Control and SAH-BRD4 cKD mice, with a greater proportion observed in the latter group (Fig. 6J-K, Fig. S5E). To ascertain changes in critical functional regions, we performed Nissl staining to evaluate the extent of neuronal damage. The results indicate that varying degrees of neuronal damage were observed in the frontal cortex (Fig. S8A-B), hippocampus (Fig. S8C-D), and tissues surrounding the puncture site (Fig. S8E-F) in the SAH-Control group of mice, and this alteration was exacerbated in the SAH-BRD4 cKD group. The survival of neurons is directly correlated with the neurological function of mice following injury. Compared with the Control group, the cKD group presented significantly lower Modified Garcia scores and Beam Balance scores after SAH (Fig. 6L-M). These findings indicate that BRD4 knockdown induces A1 polarization of reactive astrocytes, leading to increased proinflammatory cytokines and neuronal death after SAH.

Knockdown of BRD4 impaired the recovery of neurological function after SAH in mice

The recovery of neural function during the chronic injury stage is crucial for the prognosis of SAH. Twenty-eight days after SAH, long-term behavioral tests were conducted on the mice. During the rotarod test, mice in the Control group and BRD4 cKD group were able to maintain a stable grip on the rotating rod for a relatively long duration without SAH. On the first day after SAH, the time spent by the mice in the SAH-Control and SAH-BRD4 cKD groups on the beam was significantly reduced. Among them, mice in the SAH-BRD4 cKD group performed the worst. These phenomena were also observed on the 28th day (Fig. 7A). Additionally, on the 28th day, mice in the SAH-BRD4 cKD group exhibited the shortest distance traveled on the rotarod and had the lowest rotational speed (Fig. 7B-C).

Furthermore, we employed the Open Field test to further assess the locomotor and exploratory abilities of the mice. After SAH, the mice preferred to stay in the corners of the box rather than freely exploring the entire space like normal mice (Fig. 7D). In particular, the SAH-BRD4 cKD group presented the shortest distance traveled (Fig. 7E). Finally, in the Morris Water Maze test, the learning and memory abilities of the mice were evaluated

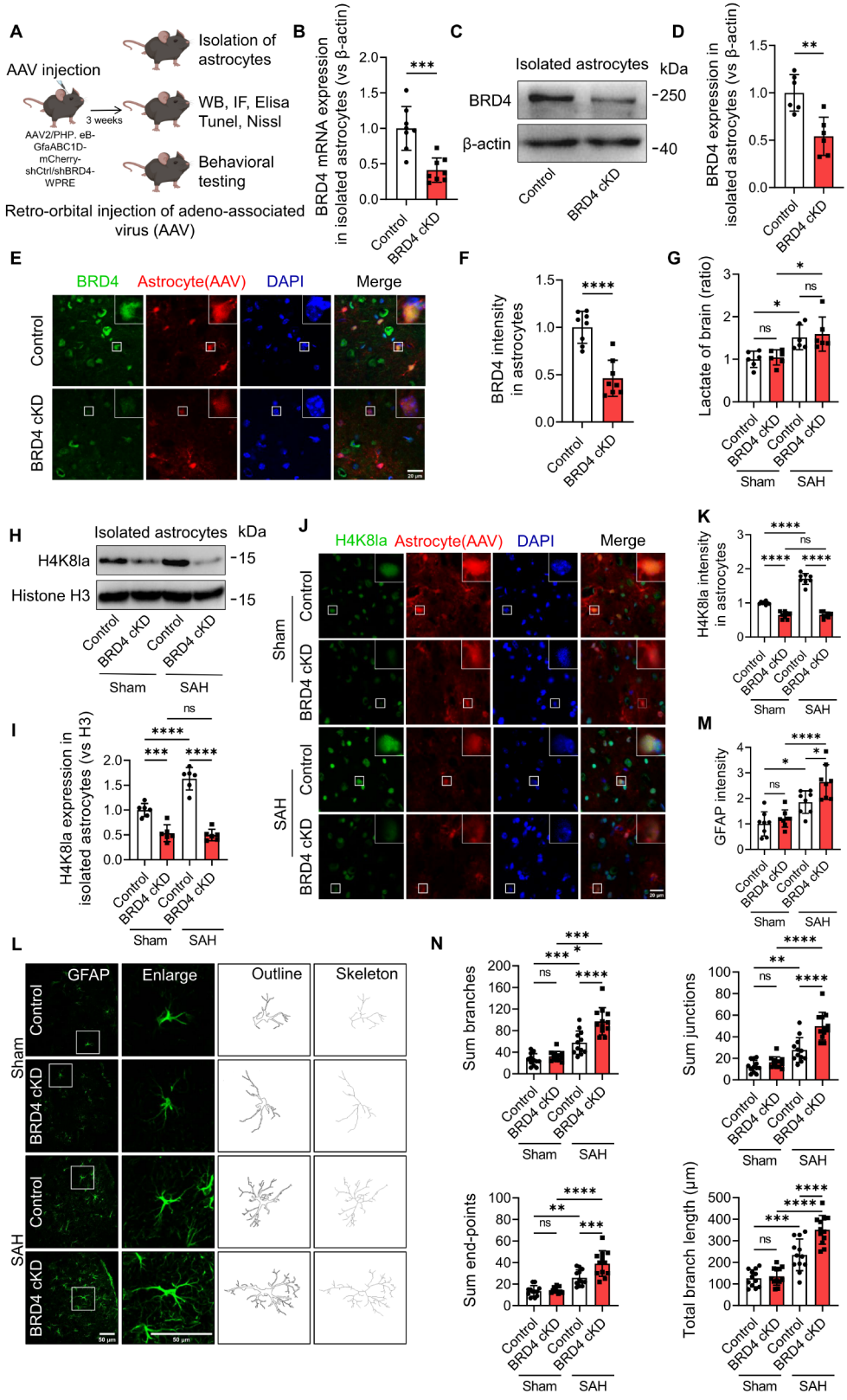

Fig. 5 (See legend on next page.)

(See figure on previous page.)

Fig. 5 Knocking down BRD4 in mouse astrocytes reduces H4K8la, thereby enhancing astrocytic reactivity. **(A)** Astrocytic BRD4 conditional knockdown (BRD4 cKD) in C57BL/6J male mice was generated via retro-orbital injection of GfaABC1D-targeting adeno-associated virus. **(B-F)** BRD4 knockdown efficiency in isolated astrocytes was determined via RT-qPCR **(B**, $n=8$), WB **(C-D**, $n=6$) and immunofluorescence **(E-F**, $n=8$ fields from 4 mice; scale bar = 20 μm). **(G)** Brain lactate concentrations were measured in Control and BRD4 cKD mice following SAH ($n=6$). **(H-I)** Representative WB images and quantification of H4K8la levels in Control and BRD4 cKD mice following SAH ($n=6$). **(J-K)** Representative fluorescent images and quantification of H4K8la levels in Control and BRD4 cKD mice following SAH ($n=8$ fields from 4 mice; scale bar = 20 μm). **(L-N)** Representative fluorescent images and quantification of GFAP intensity (M, $n=8$ fields from 4 mice; scale bar = 50 μm), sum branches, sum junctions, sum endpoints and total branch length (N, $n=12$ astrocytes from 4 mice; scale bar = 50 μm) of astrocytes in Control and BRD4 cKD mice following SAH. All values are means ± SDs, $^{*}P<0.05$, $^{**}P<0.01$, $^{***}P<0.001$, $^{****}P<0.0001$, ns, no significant changes

by analyzing their trajectories in the circular water maze (Fig. 7F). Compared with sham mice, SAH-Control mice showed no significant difference in the number of crossings through the target platform, indicating good recovery. In contrast, SAH-BRD4 cKD mice continued to exhibit low crossing frequencies, indicating impaired recovery (Fig. 7G). These data suggest that knocking down BRD4 leads to impaired recovery of learning, memory, locomotion, and balance abilities in mice during the long-term phase following SAH.

Discussion

In this study, our pivotal discoveries are as follows: (1) SAH triggered A1 polarization in astrocytes and upregulated the expression of BRD4 in astrocytes, which was accompanied by increased levels of lactate and lactylation. (2) Administration of 2-DG suppressed lactate production effectively, resulting in a subsequent reduction in astrocyte lactylation and an exacerbation of A1 polarization in OxyHb-stimulated astrocytes. Conversely, supplementation with lactate increased lactylation and attenuated A1 polarization. (3) Following SAH, BRD4 has emerged as a key modulator of A1 polarization and is strongly correlated with H4K8la, thereby affecting neuronal survival and the recovery of neural function in mice. Notably, minimal variations were observed in A2 astrocytes throughout the course of our experiments. A schematic diagram of the mechanism is shown in Fig. 8.

Astrocytes, the most numerous glial cells in the central nervous system, aid in neuronal survival, growth, and synapse formation by secreting neurotrophic and growth factors [5, 44]. Additionally, astrocytes serve as the primary energy source for neurons, ensuring their continued functionality [45]. Under pathological conditions, the astrocyte-neuron lactate shuttle has neuroprotective effects, protecting neurons from further damage [46, 47]. However, it is imperative to recognize that lactate can also have a significant effect on astrocytes. Despite extensive research, the intricate relationships among astrocyte reactivity, astrocyte polarization status, and elevated lactate levels following SAH remain unclear.

We observed an increase in lactylation in astrocytes at 24 h following SAH. Under OxyHb stimulation, treatment with 2-DG inhibited lactate production and decreased lactylation, which was accompanied by a further increase in the expression of GFAP and C3. Conversely, the addition of lactate increased lactylation and reduced the expression of GFAP and C3 in astrocytes following SAH, whereas the A2 astrocyte marker S100a10 remained relatively stable throughout these processes. We did not observe a direct correlation between lactation and A2 astrocytes. The concurrent increase in lactate levels and astrocyte A1 polarization after SAH does not conflict with our observations. This phenomenon results from the intricate and complex characteristics of astrocyte polarization, which is influenced by a range of currently unidentified mechanisms. Notably, the increase in lactate serves to provide energy for nerve cells to cope with adverse environments [14]. In addition, we discovered the regulatory role of lactate in this process.

Previous studies have indicated that increased endogenous lactate can be a factor in poor disease prognosis [16, 17]. However, recent findings have revealed a specific positive role of lactate in brain development, synaptic plasticity and angiogenesis [13, 48, 49]. Lactate not only serves as a vital energy source but also functions as a metabolic signaling molecule critical to the brain and astrocytes. It plays a central role in energy transportation, storage, production, and utilization [13]. Moreover, exogenous lactate supplementation has been demonstrated to have beneficial effects on cerebral metabolism and hemodynamics in patients with traumatic brain injury (TBI) [50]. In ischemic stroke model animals, lactate administration has been shown to attenuate inflammation by inhibiting the ubiquitination of N-Myc downstream regulated gene 2 (NDRG2) in astrocytes. Additionally, lactate reduces cell death, mitigates weight loss, and lessens the degree of ischemic damage inflicted [51–54]. We recognized the beneficial effects of lactate on astrocytes and believe that the therapeutic potential of lactate after SAH deserves further investigation.

We also observed a concurrent increase in both BRD4 and lactylation in astrocytes following SAH. Upon subsequent knockdown of BRD4 expression in astrocytes, we detected a notable decrease in histone lactylation, particularly in H4K8la levels. BRD4 and H4K8la immunoprecipitation suggested that BRD4 serves a pivotal regulatory function in H4K8la. There was no significant decrease in lactate levels in astrocytes after BRD4 knockdown, indicating that BRD4 did not affect astrocytic

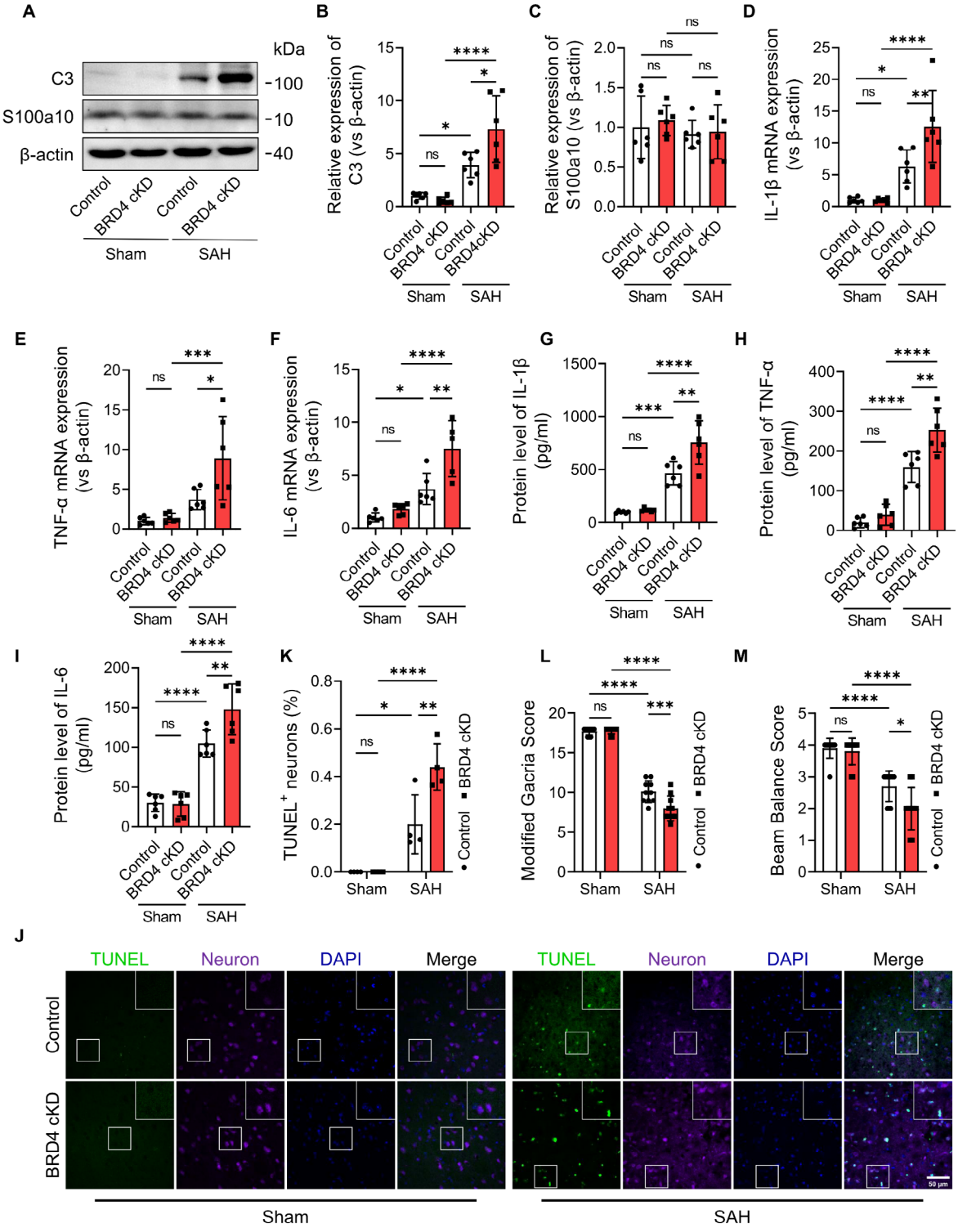

Fig. 6 Specific knocking of BRD4 in astrocytes boosts A1 astrocyte polarization, triggering inflammatory responses and neuronal death. **(A-C)** Western blot showing C3 **(B)** and S100a10 **(C)** expression of Control and BRD4 cKD mice after SAH ($n=6$). **(D-F)** mRNA levels of IL-1β, TNF-α, and IL-6 in Control and BRD4 cKD mice after SAH ($n=5$ or 6). **(G-I)** Protein levels of IL-1β, TNF-α, and IL-6 in Control and BRD4 cKD mice after SAH ($n=6$). **(J-K)** Representative fluorescent images and quantification of TUNEL$^+$ neurons of Control and BRD4 cKD mice after SAH. Nuclei were counterstained with DAPI (blue, $n=4$; scale bar = 50 μm). **(L-M)** Short-term neurological function by Modified Garcia score **(L)** and Beam Balance test **(M)**, $n=10$. All values are the mean ± SD, $^*P<0.05$, $^{**}P<0.01$, $^{***}P<0.001$, $^{****}P<0.0001$, ns, no significant changes

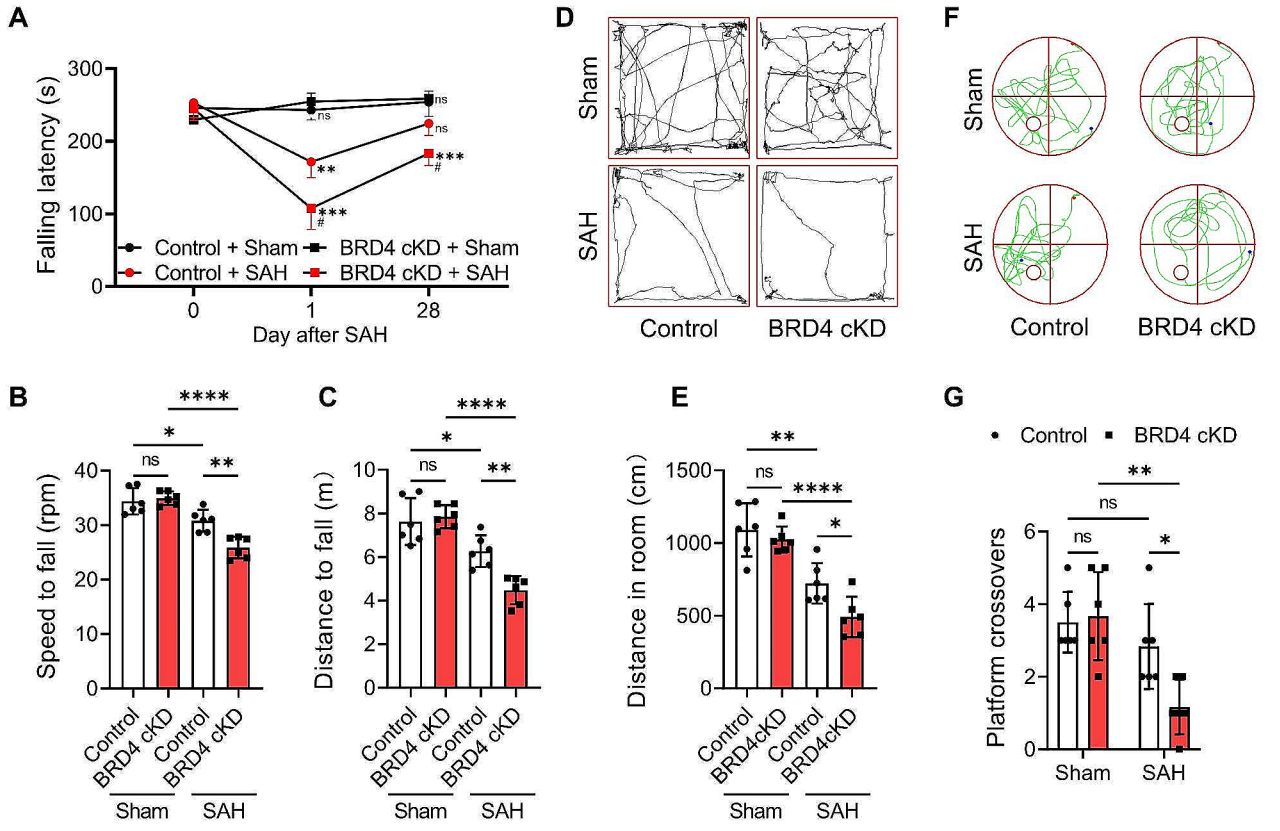

Fig. 7 BRD4 knockdown impairs neurological recovery in mice during the chronic phase following SAH. **(A-C)** Rotarod test was used to assess the falling latency **(A)**, speed to fall **(B)**, and distance to fall **(C)** of Control and BRD4 cKD mice after SAH ($n=6$). **(D-E)** Representative trajectory maps and statistical results from the Open field test ($n=6$). **(F-G)** Representative trajectory maps and platform crossovers from the Morris Water Maze test ($n=6$). All values are mean ± SD, *$P<0.05$, **$P<0.01$, ***$P<0.001$, ****$P<0.0001$, ns, no significant changes

glycolysis. As mentioned earlier, BRD4, which serves as both a transcription factor and an epigenetic factor, is involved in the regulation of acetylation and methylation [24, 55, 56]. Coincidentally, our results also revealed that BRD4 performs a comparable regulatory role in lactylation, thereby contributing further to the elucidation of the diverse functions of BRD4.

The histone H4K8 is highly important in the central nervous system. Recent studies have firmly established that the increase in MAP-2 expression, achieved through the modulation of H4K8 acetylation, can effectively mitigate the harmful effects of cerebral ischemia-reperfusion injury [57]. H4K8la is considered to be closely related to embryonic development [58]. Our study revealed that silencing BRD4 significantly reduced H4K8la levels and exacerbated A1 polarization and inflammatory responses in astrocytes. The release of neurotoxic substances by A1 astrocytes, which triggers neuronal death, is intricately associated with the severity and prognosis of SAH [59, 60].

The pivotal role of BRD4 in the central nervous system is beyond question [25]. The absence of BRD4 impairs critical synaptic proteins, leading to memory deficits in mice [26]. In addition to its neuroprotective role, studies have reported that inhibiting BRD4 function can alleviate inflammatory and other adverse reactions [31, 61]. Furthermore, numerous studies have pointed to the beneficial role of BRD4 in maintaining normal functions. BRD4 orchestrates genome folding to promote neural crest differentiation, and BRD4 deletion in the neural crest results in cohesinopathy-like phenotypes [32]. Deletion of BRD4 in adult mice leads to acute deterioration of cardiac contractile function [62]. Using an inducible BRD4 knockout mouse model, researchers have demonstrated that deletion of BRD4 ($BRD4^{\Delta/\Delta}$) in the hematopoietic system impairs hematopoietic stem cell (HSC) self-renewal and differentiation, which is associated with H3 clipping [63]. A comprehensive exploration of astrocyte BRD4 function is imperative to further clarify the neuroprotective molecular mechanisms underlying BRD4 in SAH.

We provided the mice with an optimized living environment and a diet with a scientifically established nutrition formula. We used small surgical incisions, which can reduce the additional damage. Simultaneously, strictly monitoring body temperature, respiration, and heart rate during surgery, positioning the mice correctly and

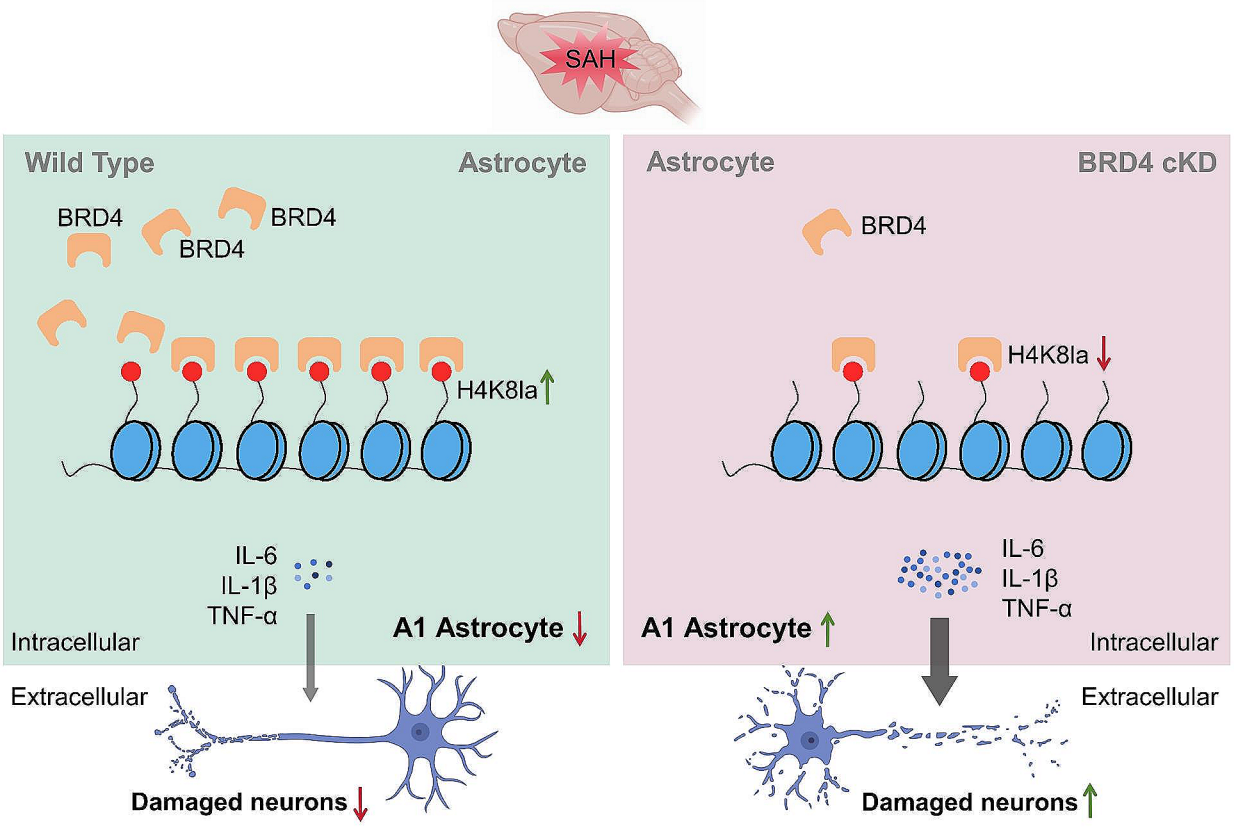

Fig. 8 BRD4-mediated histone lactylation regulates astrocyte polarization after experimental SAH. After SAH, astrocytes undergo polarization toward the neurotoxic A1 phenotype. BRD4 mitigates the A1 polarization of astrocytes via H4K8la. However, when BRD4 is knocked down, H4K8la levels are significantly reduced, subsequently leading to the exacerbation of A1 polarization in astrocytes. This, in turn, enhances the marked release of proinflammatory factors, including IL-6, IL-1β, and TNF-α, ultimately resulting in neuronal death

maintaining a clear respiratory tract after surgery may reduce mortality rates when establishing this model.

Notably, there are differences in the fluorescence intensity, number of branches, junction points, endpoints, and branch length of astrocytes in different brain regions (frontal cortex, hippocampus, and tissues surrounding the puncture site) under Sham and SAH conditions, which may be related to the different functional roles of astrocytes in these regions. In the future, it is worth conducting further extensive experiments to further investigate this finding.

There are several limitations in our research. First, our study focused exclusively on both animals and cells, specifically on astrocytes, and focused on the A1 polarization of astrocytes after BRD4 knockdown. Future experiments will involve overexpression or similar interventions to further refine and strengthen our findings. Second, although we have been established that BRD4 regulates astrocyte polarization post-SAH through histone lactylation, the intricacies underlying this process remain mostly unmapped and unexplored. Finally, our current study was confined to male mice, thereby potentially introducing constraints in the generalization of our findings. Therefore, the sex aspect deserves further exploration and refinement in future studies.

In conclusion, our research shows that BRD4 regulates lactylation and has a significant effect on the polarization of astrocytes after SAH. This regulatory mechanism is intricately linked to H4K8la, suggesting a novel perspective on the dysfunctional state of astrocytes following SAH. Future investigations will delve deeper into the precise mechanisms by which BRD4 and lactylation regulate astrocyte polarization, providing us with more nuanced and precise information that could inform the development of more effective therapeutic strategies.

Abbreviations

AAV Adeno	Associated virus
ACM	Astrocyte-conditioned medium
BRD4	Bromodomain-containing protein 4
B3gnt5	β1, 3-N-acetylglucosaminyltransferase 5
C3	Complement 3
Clcf1	Cardiotrophin-like cytokine factor 1
Elisa	Enzyme-linked immunosorbent assay
GFAP	Glial fibrillary acidic protein
Gbp2	Guanylate-binding protein 2
IL-6	Interleukin 6

IL-1β	Interleukin-1β
IP	Immunoprecipitation
Pan-Kla	Pan-lysine lactylation
S100a10	S100 calcium-binding protein a10
Serping1	Serpin family G member 1
SAH	Subarachnoid hemorrhage
Tm4sf1	Transmembrane 4 L six family member 1
TNF-α	Tumor necrosis factor α
Ugt1a1	Uridine diphosphate glucuronosyl transferase 1a1

Supplementary Information

The online version contains supplementary material available at https://doi.org/10.1186/s12974-024-03185-6.

Supplementary Material 1

Author contributions

F.Z., Y.J. and J.H.P. designed the experiments. F.Z., J.Z., P.L., X.H.Z., L.Y., J.P.W., L.H.Z., L.F.Z., J.W.P, H.F.X. and B.Q.X. performed the experiments. F.Z., J.Z. and P.L. analyzed raw data. Y.J. and J.H.P. reviewed the data and made substantial contributions to improving the studies. F. Z. and J.H.P. wrote the manuscript. All the authors have contributed to the critical revision of the final manuscript.

Funding

This work was supported by grants from the National Natural Science Foundation of China (82371310, 82271306), the Sichuan Science and Technology Support Program (2023YFH0069, 2023NSFSC0028, 2022YFS0615, 2023NSFSC1559, 2022NSFSC1421) and the Scientific Research Project of the Sichuan Provincial Health Commission (23LCYJ040), and the Youth Foundation of Southwestern Medical University and Southwest Medical University Project (2020ZRQNB072, 2021ZKZD013, 2021LZXNYD-P01, 2023QN014, 2022-JYJ-158).

Data availability

No datasets were generated or analysed during the current study.

Declarations

Ethics approval

All procedures involving research animals were conducted Animal Committee of the Ethics Committee of Southwest Medical University (Approval Number: 20220223-010), and were performed in accordance with the National Institutes of Health guidelines for the Care and Use of Laboratory Animals.

Competing interests

The authors declare no competing interests.

Received: 21 April 2024 / Accepted: 24 July 2024
Published online: 30 July 2024

References

1. Etminan N, Chang HS, Hackenberg K, et al. Worldwide Incidence of Aneurysmal Subarachnoid Hemorrhage according to Region, Time Period, blood pressure, and Smoking Prevalence in the Population: a systematic review and Meta-analysis. JAMA Neurol. 2019;76(5):588–97.
2. Claassen J, Park S. Spontaneous subarachnoid haemorrhage. Lancet. 2022;400(10355):846–62.
3. Chen X, Giles J, Yao Y, et al. The path to healthy ageing in China: a Peking University-Lancet Commission. Lancet. 2022;400(10367):1967–2006.
4. Bonvento G, Bolanos JP. Astrocyte-neuron metabolic cooperation shapes brain activity. Cell Metab. 2021;33(8):1546–64.
5. Allen NJ, Lyons DA. Glia as architects of central nervous system formation and function. Science. 2018;362(6411):181–5.
6. Patani R, Hardingham GE, Liddelow SA. Functional roles of reactive astrocytes in neuroinflammation and neurodegeneration. Nat Rev Neurol. 2023;19(7):395–409.
7. Wang C, Li L. The critical role of KLF4 in regulating the activation of A1/A2 reactive astrocytes following ischemic stroke. J Neuroinflammation. 2023;20(1):44.
8. Nakano-Kobayashi A, Canela A, Yoshihara T, et al. Astrocyte-targeting therapy rescues cognitive impairment caused by neuroinflammation via the Nrf2 pathway. Proc Natl Acad Sci U S A. 2023;120(33):e2303809120.
9. Yun SP, Kam TI, Panicker N, et al. Block of A1 astrocyte conversion by microglia is neuroprotective in models of Parkinson's disease. Nat Med. 2018;24(7):931–8.
10. Guttenplan KA, Weigel MK, Prakash P, et al. Neurotoxic reactive astrocytes induce cell death via saturated lipids. Nature. 2021;599(7883):102–7.
11. Zhang L, Guo K, Zhou J, et al. Ponesimod protects against neuronal death by suppressing the activation of A1 astrocytes in early brain injury after experimental subarachnoid hemorrhage. J Neurochem. 2021;158(4):880–97.
12. Xiong XY, Tang Y, Yang QW. Metabolic changes favor the activity and heterogeneity of reactive astrocytes. Trends Endocrinol Metab. 2022;33(6):390–400.
13. Wu A, Lee D, Xiong WC, Lactate Metabolism. Signaling, and function in Brain Development, synaptic plasticity, angiogenesis, and neurodegenerative diseases. Int J Mol Sci 2023, 24(17).
14. Chamaa F, Magistretti PJ, Fiumelli H. Astrocyte-derived lactate in stress disorders. Neurobiol Dis. 2024;192:106417.
15. Magistretti PJ, Allaman I. Lactate in the brain: from metabolic end-product to signalling molecule. Nat Rev Neurosci. 2018;19(4):235–49.
16. Radolf S, Smoll N, Drenckhahn C, et al. Cerebral lactate correlates with early onset pneumonia after aneurysmal SAH. Transl Stroke Res. 2014;5(2):278–85.
17. Aisiku IP, Chen PR, Truong H, et al. Admission serum lactate predicts mortality in aneurysmal subarachnoid hemorrhage. Am J Emerg Med. 2016;34(4):708–12.
18. Bouzat P, Oddo M. Lactate and the injured brain: friend or foe? Curr Opin Crit Care. 2014;20(2):133–40.
19. Zhang D, Tang Z, Huang H, et al. Metabolic regulation of gene expression by histone lactylation. Nature. 2019;574(7779):575–80.
20. Xiong J, He J, Zhu J, et al. Lactylation-driven METTL3-mediated RNA m(6)a modification promotes immunosuppression of tumor-infiltrating myeloid cells. Mol Cell. 2022;82(9):1660–e167710.
21. Fan M, Yang K, Wang X, et al. Lactate promotes endothelial-to-mesenchymal transition via Snail1 lactylation after myocardial infarction. Sci Adv. 2023;9(5):eadc9465.
22. Pan RY, He L, Zhang J, et al. Positive feedback regulation of microglial glucose metabolism by histone H4 lysine 12 lactylation in Alzheimer's disease. Cell Metab. 2022;34(4):634–48. e6.
23. Zhou J, Zhang L, Peng J et al. Astrocytic LRP1 enables mitochondria transfer to neurons and mitigates brain ischemic stroke by suppressing ARF1 lactylation. Cell Metabol 2024, (36):1–15.
24. Singh MB, Sartor. G C BET bromodomains as novel epigenetic targets for brain health and disease. Neuropharmacology. 2020;181:108306.
25. Liu L, Yang C, Candelario-Jalil E. Role of BET Proteins in inflammation and CNS diseases. Front Mol Biosci. 2021;8:748449.
26. Korb E, Herre M, Zucker-Scharff I, et al. BET protein Brd4 activates transcription in neurons and BET inhibitor Jq1 blocks memory in mice. Nat Neurosci. 2015;18(10):1464–73.
27. Muhar M, Ebert A, Neumann T, et al. SLAM-seq defines direct gene-regulatory functions of the BRD4-MYC axis. Science. 2018;360(6390):800–5.
28. Moudgil A, Wilkinson MN, Chen X, et al. Self-reporting transposons enable simultaneous readout of Gene expression and transcription factor binding in single cells. Cell. 2020;182(4):992–e100821.
29. Wang N, Wang W, Wang X, et al. Histone lactylation boosts reparative gene activation post-myocardial infarction. Circ Res. 2022;131(11):893–908.
30. Wang X, Fan W, Li N, et al. YY1 lactylation in microglia promotes angiogenesis through transcription activation-mediated upregulation of FGF2. Genome Biol. 2023;24(1):87.
31. Liu L, Yang C, Lavayen BP, et al. Targeted BRD4 protein degradation by dBET1 ameliorates acute ischemic brain injury and improves functional outcomes associated with reduced neuroinflammation and oxidative stress and preservation of blood-brain barrier integrity. J Neuroinflammation. 2022;19(1):168.
32. Linares-Saldana R, Kim W, Bolar NA, et al. BRD4 orchestrates genome folding to promote neural crest differentiation. Nat Genet. 2021;53(10):1480–92.
33. Yardeni T, Eckhaus M, Morris HD, et al. Retro-orbital injections in mice. Lab Anim (NY). 2011;40(5):155–60.
34. Prabhakar S, Lule S, da Hora CC, et al. AAV9 transduction mediated by systemic delivery of vector via retro-orbital injection in newborn, neonatal and juvenile mice. Exp Anim. 2021;70(4):450–8.

35. Peng J, Wu Y, Pang J, et al. Single clip: an improvement of the filament-perforation mouse subarachnoid haemorrhage model. Brain Inj. 2019;33(6):701–11.
36. Zhang Y, Yang X, Ge X, et al. Puerarin attenuates neurological deficits via Bcl-2/Bax/cleaved caspase-3 and Sirt3/SOD2 apoptotic pathways in subarachnoid hemorrhage mice. Biomed Pharmacother. 2019;109:726–33.
37. Nakano F, Kanamaru H, Kawakita F, et al. Epidermal growth factor receptor mediates neuronal apoptosis after subarachnoid hemorrhage in mice. Stroke. 2023;54(6):1616–26.
38. Tao Q, Qiu X, Li C, et al. S100A8 regulates autophagy-dependent ferroptosis in microglia after experimental subarachnoid hemorrhage. Exp Neurol. 2022;357:114171.
39. Kim S, Kwon SH, Kam TI, et al. Transneuronal Propagation of pathologic alpha-synuclein from the gut to the Brain models Parkinson's Disease. Neuron. 2019;103(4):627–41. e7.
40. Chung DY, Oka F, Jin G, et al. Subarachnoid hemorrhage leads to early and persistent functional connectivity and behavioral changes in mice. J Cereb Blood Flow Metab. 2021;41(5):975–85.
41. Xu P, Tao C, Zhu Y, et al. TAK1 mediates neuronal pyroptosis in early brain injury after subarachnoid hemorrhage. J Neuroinflammation. 2021;18(1):188.
42. Chandra S, Di Meco A, Dodiya HB, et al. The gut microbiome regulates astrocyte reaction to Abeta amyloidosis through microglial dependent and independent mechanisms. Mol Neurodegener. 2023;18(1):45.
43. Young K, Morrison H. Quantifying Microglia Morphology from Photomicrographs of Immunohistochemistry Prepared Tissue Using ImageJ. J Vis Exp 2018, (136).
44. Santello M, Toni N, Volterra A. Astrocyte function from information processing to cognition and cognitive impairment. Nat Neurosci. 2019;22(2):154–66.
45. Belanger M, Allaman I, Magistretti PJ. Brain energy metabolism: focus on astrocyte-neuron metabolic cooperation. Cell Metab. 2011;14(6):724–38.
46. Sun Y, Wang Y, Chen ST et al. Modulation of the Astrocyte-Neuron Lactate Shuttle System contributes to Neuroprotective action of Fibroblast Growth Factor 21. Theranostics. 2020, 10(18):8430–8445.
47. Takahashi S. Neuroprotective function of high glycolytic activity in astrocytes: common roles in stroke and neurodegenerative diseases. Int J Mol Sci 2021, 22(12).
48. Margineanu MB, Mahmood H, Fiumelli H, et al. L-Lactate regulates the expression of synaptic plasticity and neuroprotection genes in cortical neurons: a transcriptome analysis. Front Mol Neurosci. 2018;11:375.
49. Morland C, Andersson KA, Haugen OP, et al. Exercise induces cerebral VEGF and angiogenesis via the lactate receptor HCAR1. Nat Commun. 2017;8:15557.
50. Bouzat P, Sala N, Suys T, et al. Cerebral metabolic effects of exogenous lactate supplementation on the injured human brain. Intensive Care Med. 2014;40(3):412–21.
51. Xu J, Ji T, Li G, et al. Lactate attenuates astrocytic inflammation by inhibiting ubiquitination and degradation of NDRG2 under oxygen-glucose deprivation conditions. J Neuroinflammation. 2022;19(1):314.
52. Buscemi L, Price M, Castillo-Gonzalez J et al. Lactate Neuroprotection against transient ischemic brain Injury in mice appears Independent of HCAR1 activation. Metabolites 2022, 12(5).
53. Horn T, Klein J. Neuroprotective effects of lactate in brain ischemia: dependence on anesthetic drugs. Neurochem Int. 2013;62(3):251–7.
54. Zhao Y, Zhang X, Chen X et al. Neuronal injuries in cerebral infarction and ischemic stroke: from mechanisms to treatment (review). Int J Mol Med 2022, 49(2).
55. Mills RJ, Humphrey SJ, Fortuna PRJ, et al. BET inhibition blocks inflammation-induced cardiac dysfunction and SARS-CoV-2 infection. Cell. 2021;184(8):2167–e218222.
56. Nicodeme E, Jeffrey KL, Schaefer U, et al. Suppression of inflammation by a synthetic histone mimic. Nature. 2010;468(7327):1119–23.
57. Ma H, Hu ZC, Long Y, et al. Tanshinone IIA Microemulsion protects against Cerebral Ischemia Reperfusion Injury via regulating H3K18ac and H4K8ac in vivo and in Vitro. Am J Chin Med. 2022;50(7):1845–68.
58. Yang D, Zheng H, Lu W et al. Histone lactylation is involved in mouse oocyte maturation and embryo development. Int J Mol Sci 2024, 25(9).
59. Liang P, Zhang X, Zhang Y, et al. Neurotoxic A1 astrocytes promote neuronal ferroptosis via CXCL10/CXCR3 axis in epilepsy. Free Radic Biol Med. 2023;195:329–42.
60. Liddelow SA, Guttenplan KA, Clarke LE, et al. Neurotoxic reactive astrocytes are induced by activated microglia. Nature. 2017;541(7638):481–7.
61. Zhou Y, Gu Y, Liu J. BRD4 suppression alleviates cerebral ischemia-induced brain injury by blocking glial activation via the inhibition of inflammatory response and pyroptosis. Biochem Biophys Res Commun. 2019;519(3):481–8.
62. Padmanabhan A, Alexanian M, Linares-Saldana R, et al. BRD4 (bromodomain-Containing protein 4) interacts with GATA4 (GATA binding protein 4) to govern mitochondrial homeostasis in adult cardiomyocytes. Circulation. 2020;142(24):2338–55.
63. Yang H, Sui P, Guo Y, et al. Loss of BRD4 induces cell senescence in HSC/HPCs by deregulating histone H3 clipping. EMBO Rep. 2023;24(10):e57032.

Publisher's Note